J Appl Electrochem (2009) 39:2129–2141
DOI 10.1007/s10800-009-9932-0

ORIGINAL PAPER

Conductivity studies of sol-gel prepared $BaCe_{0.85-x}Zr_xY_{0.15}O_{3-\delta}$ solid electrolytes using impedance spectroscopy

L. Doubova · S. Barison · S. Boldrini · M. Fabrizio · C. Mortalò · C. Pagura

Received: 8 October 2008 / Accepted: 12 May 2009 / Published online: 7 July 2009

Abstract A systematic investigation on doped barium cerate perovskites on conductivity was performed by means of ac electrochemical impedance spectroscopy technique. $BaCe_{0.85-x}Zr_xY_{0.15}O_{3-\delta}$ powders ($x = 0$, 0.1, 0.2, 0.3, 0.4) were prepared by a modified sol-gel Pechini method and sintered at 1,250 °C–1,450 °C, depending on Zr content, to obtain good densities (93–97% of the theoretical ones). The measured total conductivities for these solid solutions in three different atmospheres were reported: in dry oxygen, in dry nitrogen and wet (0.5 bar H_2O) hydrogen (5%H_2/Ar) atmospheres. Arrhenius plots recorded in dry oxygen as well as in dry nitrogen showed some residual hydration which remained in the specimens upon initial heating. The compositions with $x = 0.3$ and 0.4 gave conductivities close to 10^{-2} S/cm in 5%H_2/Ar/H_2O atmosphere at 600 °C. The isothermal conductivities values showed a little variation for x from 0.2 to 0.4 between 500 and 800 °C.

Keywords Proton conductivity · Sol-gel · Zr-substituted $BaCeO_3$ · Intermediate Temperature Solid Oxide Fuel Cell (IT-SOFC)

L. Doubova (✉) · S. Barison · M. Fabrizio · C. Mortalò · C. Pagura
Istituto per l'Energetica e le Interfasi (IENI), Consiglio Nazionale delle Ricerche (CNR), Corso Stati Uniti 4, 35127 Padova, Italy
e-mail: l.doubova@ieni.cnr.it

S. Boldrini
ISIB-CNR, Corso Stati Uniti 4, 35127 Padova, Italy

1 Introduction

One of the approaches to the lowering of solid oxide fuel cell (SOFC) operating temperatures by means of new electrolyte materials is the use of high temperature protonic conductors. Doped ABO_3 oxides with perovskite structures have collected much attention as promising candidates for the substitution of yttria-stabilized zirconia in the development of intermediate temperatures SOFCs [1–8]. Various doped $BaCeO_3$ compounds showed high proton conductivity, which is about one order of magnitude larger than that of ionic conductor yttria-stabilized zirconia at 500 °C. The electrical conductivity and the stability under oxidative and reductive atmospheres for doped $BaCeO_3$ are greatly dependent on the kind and quantity of doping elements and on the synthetic method of preparation. Several groups have investigated electrical conductivity in Y-doped $BaCeO_3$ as well as Y-doped $BaZrO_3$. The reported electrical conductivity values, however, vary over a wide range. The classical solid state reaction route usually needs high sintering temperature about 1,400–1,700 °C. The new synthetic methods and properties of the obtained solid solutions were actively studied in the last years [9–15]. Thus high and reproducible densities (up to ~97–99%) were obtained for Ce-based ceramics with sub-micrometric powders [13–17]. The sub-micrometric powder preparation can additionally gives certain technological advantages connected with high activity of the nano-sized powders used. The sintering temperature of high activity nano-sized powders is about 100–400 °C lower than that of solid state prepared ceramics, which indicate a more rapid processes of their sintering, thus making possible to produce materials with a fine microstructure. Together with benefits, the fine-grained solid solutions have a developed inter-crystalline

boundary, whose properties are likely to substantially affect the charge transport. Moreover, depending on the material quality, opposite effects are possible. On one hand, boundaries of grains possess an elevated concentration of point defects, which is beneficial for ionic transport and may lead to an increase in electro-conductivity; on the other hand the imperfections of inter-grain contacts (impurities, nano-sized pores) exert a negative effect on the charge transport. Among various methods recently proposed to synthesize nano-crystalline powders, the modified Pechini method has the advantage to produce high purity and ultrafine powders. In previous investigations [6, 18, 19] we found that yttrium doped barium cerates ($BaCe_{1-y}Y_yO_3$ with $y = 0.1$, 0.15, and 0.2) prepared by means of sol-gel route employing a barium excess gave high active nano-sized powders and sub-micrometric solid solutions. Sintering temperatures of 1,250 °C for $BaCeYO_{3-\delta}$ resulted in high densities. The measured total conductivities for these solid solutions in wet hydrogen atmosphere were in good agreement with reported data [6] confirming that the sol-gel synthesized $BaCe_{1-y}Y_yO_{3-\delta}$ materials are promising high protonic conductor solid electrolytes for intermediate temperature electrochemical devices. However, the chemical stability in CO_2 and H_2O environments indicated that $BaCeYO_{3-\delta}$ solid electrolytes are not sufficiently structurally stable [20, 21]. Partial substitution of Ce with Zr in perovskite oxide powders increases their chemical stability in CO_2 atmosphere starting from 20% Zr [17, 19]. Since $BaCeO_3$ and $BaZrO_3$ can easily form solid solution, it is possible to replace any desired fraction of the Ce in $BaCeO_3$ with Zr, and solid solution between cerate and zirconate should have both high protonic conductivity and good chemical stability.

Based on the discussion above, recently $BaCe_{1-x-y}Zr_xY_yO_{3-\delta}$ solid solutions were prepared by means of both solid state ($BaCe_{0.8-x}Zr_xY_{0.2}O_{3-\delta}$ (from $x = 0$ to $x = 0.8$)) [17] and $BaCe_{1-x-y}Zr_xY_yO_{3-\delta}$ Pechini methods (from $x = 0$ to $x = 0.8$) [16]. High density pellet were obtained after the sintering at temperatures of 1,300–1,450 °C [19], and 1,550–1,650 °C [16, 17] depending on Zr content due to the difficulties in their densification.

Since, a solid proton conductor that combines the high chemical stability of zirconates and the high conductivity of the cerates is very interesting to study, in this work the effect of Zr- doping in $BaCe_{1-x-y}Zr_xY_yO_{3-\delta}$ solid solutions on conductivity at low (100–250 °C) and high (300–700 °C) temperature range was investigated. The gas atmospheres used in this work were selected in order to examine in turn of high and low partial pressure of three electroactive species—oxygen, hydrogen and water.

2 Experimental

2.1 Specimens preparation

Nano-sized powder of solid electrolytes $BaCe_{0.85-x}Zr_xY_{0.15}O_{3-\delta}$ with a variable Zr concentration x, ($x = 0$, 0.1, 0.2, 0.3, 0.4), were prepared by a modified sol-gel Pechini method using EDTA and ethylene glycol as a complexing and polymerizing agents to produce high surface area reactive ceramic powders. The average particle sizes were about 0.1–0.3 micron. The preparation of specimens was similar to that in previous studies [6, 18]. The resulting materials were characterized by various techniques. The density was determined by measurements of pellet mass and dimension after sintering. The density of the specimens was $\approx$93–97% of the theoretical ones based on crystal lattice parameters. The stoichiometry was determined by quantitative analysis via electron microprobe and showed differences not over 5% for Ce, Zr and Y indicating a Ba vaporization during sintering of about $6 \div 10\%$. The results of this analysis are reported in [18]. As it was proposed in [19], 10 mol% barium excess was added to all the compositions. The powder X-ray patterns [18, 19] confirmed that the materials were single-phase perovskites. Fine $BaCe_{1-x}Zr_xY_{0.15}O_{3-\delta}$ powders were obtained by calcination in air for 6 h (heating rate 9 °C/min) at temperatures ranging between 1,100 and 1,250 °C, depending on Zr content. Powders were uniaxially dry pressed in form of rectangular specimens at 700 MPa. The average effective diameter of grains in sintered pellets was estimated from SEM images about $0.8 \div 1.2$ μm. Reported in [18, 19] SEM micrographs of sintered pellets confirmed good coarsening and highly dense materials.

2.2 Electrical measurements

The study of the conductivity performance of the $BaCe_{0.85-x}Zr_xY_{0.15}O_{3-\delta}$ solid solutions in oxidative and reductive conditions was performed with the ac electrochemical impedance spectroscopy technique.

Impedance spectra were obtained using Autolab PGSTAT100 from 1 Hz to 1 MHz with 60 logarithmically spaced data points. The temperature was increased from 100 to 900 °C (50 °C/interval) with particular attention to ensure equilibrium conditions at each point. All impedance spectra presented here were obtained using a two-electrode cell configuration under symmetrical cell conditions, with platinum electrodes sputtered onto the surfaces of the specimens, and were analyzed by using the Zview2 modelling software (Scribner Associates, Inc.). The impedance spectra were collected in atmospheres of dry and wet ($P_{H_2O} = 0.5$ bar) oxygen, nitrogen and 5% hydrogen/argon. Dry oxygen and nitrogen were used without any

treatment (H_2O content <0.5 ppm). Wet atmospheres were prepared by using a Controlled Evaporator Mixer (Bronkhorst High-Tech B.V.). Total flow rate was 100 mL/min. In wet 5% H_2/Ar conditions the impedance responses of the $BaCe_{1-x}Zr_xY_{0.15}O_{3-\delta}$ pellets were recorded after ~20 min water vapour introduction into flowing gas at 100 °C. The results are corrected for sample geometry leading to apparent conductivity data. A further correction was applied in order to obtain specific grain boundary conductivity.

2.2.1 *Impedance spectroscopy analysis*

The electric properties as a function of the frequency of the material were determinate with impedance spectroscopy. This allowed to distinct among the different conducting process. Charge transfer process at the electrodes, measured at low frequencies, can be separated from ion conduction in the material. In addition, distinction can be made between conductivity in the grain interior at high frequencies and ion conduction in grain boundaries at lower frequencies. The simple semi-empirical Debye-type model as well as accurate fitting via non-linear least squares of constant-phase elements were used; both Unit-Weight and Calc-Modulus approximations [22] were used to obtain RC parameters (R is the resistance, C is the capacitance) of the solid electrolyte material which are straightforward to components of the microstructure. In addition of C and R, f_{rel} and τ (f_{rel} is relaxation frequency and τ is the time constant) were extracted [23]. Measuring of f_{rel} and its temperature or composition dependences may be particularly useful in comparing samples which have different geometries, different microstructures or have been prepared in different way. Moreover, relaxation time analysis will become particularly helpful in more difficult systems (technical electrode structures) where the distribution function of relaxation times may be used as pre-identification method for a detail modelling of the complex interfacial geometries [24].

3 Results and discussion

3.1 Overview

It was accepted after Iwahara [1, 2] that protonic conductive material incorporates protons through the Wagner reaction (Eq. 1) with water vapour and retained their proton conductivity up to high temperature.

$$H_2O + V_O^{\bullet\bullet} + O_O^x \leftrightarrow 2OH_O^{\bullet} \quad (1)$$

This reaction, which occurs at any free surface of the ceramic exposed to the water vapour, has an equilibrium constant:

$$K_w(T) = \left[OH^{\bullet}\right]^2 \Big/ \left[V_O^{\bullet\bullet}\right] p_{H_2O} \left[O_o^x\right] \quad (2)$$

Ionic transport through the electrolyte solid solution depends on several factors, many of which are interdependent. Moreover, either hydration or dehydration may occur depending on local partial pressure of water vapour and value of the equilibrium constant, since the Wagner reaction is thermodynamically reversible. Thus, under fuel cell conditions with the sample exposed to hydrogen and to air/oxygen, the concentration of proton should be increased also due to high activity of water vapour in the protonic electrolyte.

The total conductivity of proton conductive materials is the sum of the partial conductivities of electrons, holes, protonic defects and oxygen ion vacancies [25].

3.1.1 *Conductivity of $BaCe_{0.85-x}Zr_xY_{0.15}O_{3-\delta}$ in dry gas atmospheres of oxygen and nitrogen*

In dry air or oxygen, conductivity of doped mixed oxides is supposed to be only due to combination of holes and oxygen ion vacancies since the concentration of protonic defects is small at low p_{H_2O}. In fact, at high oxygen pressure, oxygen may reacts with available oxygen ion vacancies at the surface, generating electron holes. When the used gas has relatively low pO_2 the diffusion limitation of oxygen molecules or O atoms limits the electron holes generation.

The typical examples of the total conductivities (σ_{total}) for $BaCe_{0.75}Zr_{0.1}Y_{0.15}$ recorded in 100–900° temperature range in flowing dry O_2 and dry N_2 atmospheres are shown in Fig. 1a, b, in which the data are plotted in the Arrhenius form.

$$\sigma = \frac{\sigma_0}{T} \cdot e^{-E_a/kT} \quad (3)$$

where σ is the conductivity, σ_0 is the pre-exponential factor, T is the absolute measurement temperature, k is Boltzman constant and E_a is the activation energy for conduction. The electrical conductivities could be calculated in two ways. The first is to convert the resistance to the conductivity by consideration of sample geometry:

$$\sigma_{tot} = \frac{l}{A} \cdot \frac{1}{R_1 + R_2} \quad (4)$$

$$\sigma_{bulk} = \frac{l}{A} \cdot \frac{1}{R_1} \quad (5)$$

where l is the sample thickness, A is the sample area, R_1 and R_2 are the resistance of the bulk and of the grain boundary. This simple model was applied for the total and bulk conductivity calculations in oxygen, nitrogen and 5%H_2/Ar atmospheres (Fig. 1a, b, 3a, 6a). A further correction could be made in order to obtain specific

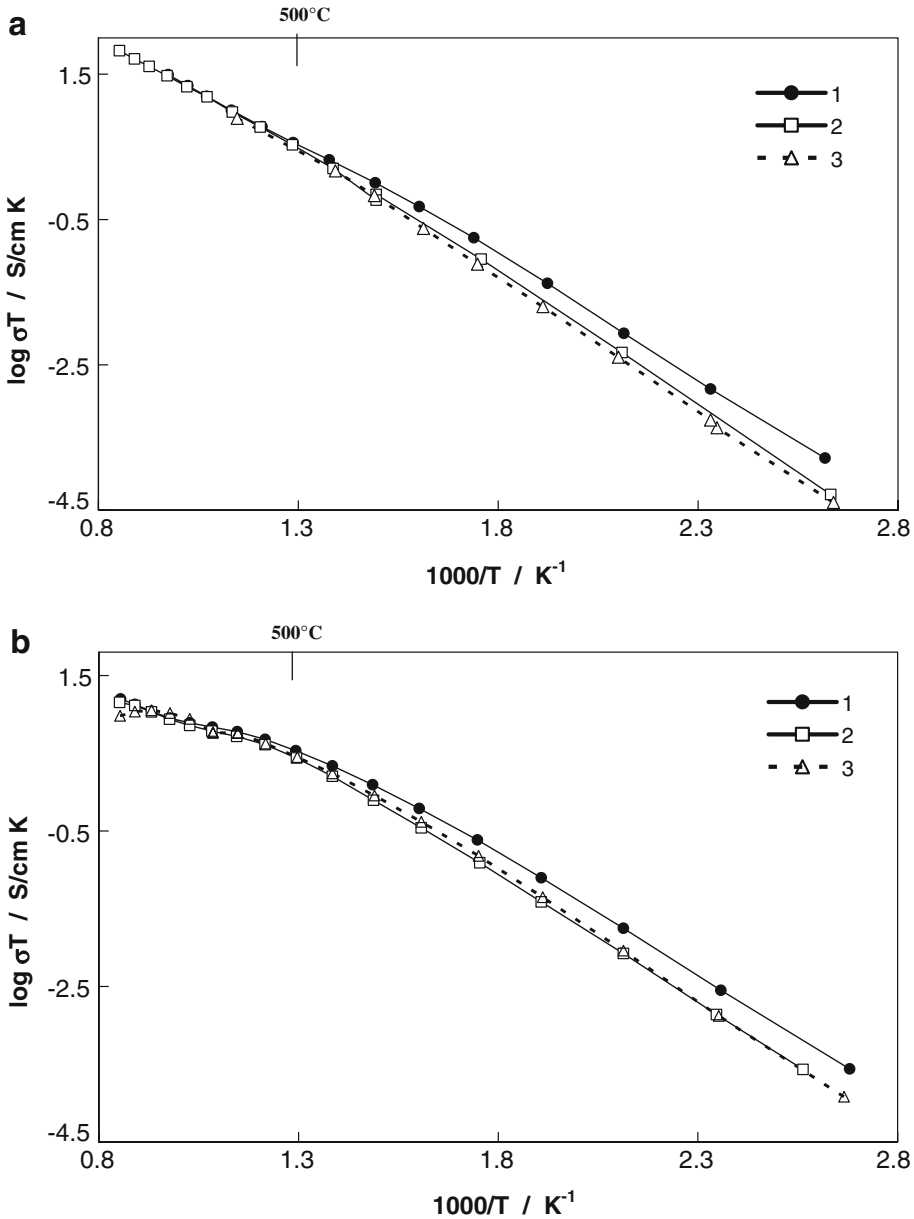

Fig. 1 Arrhenius plots of total conductivity for the $BaCe_{0.75}Zr_{0.1}Y_{0.15}O_3$ solid solutions measured in **a** dry oxygen and **b** dry nitrogen atmospheres: (1) first heating (2) second heating, (3) third heating in a humidified atmospheres ($P_{H_2O} = 0.5$ bar)

conductivity as it will be applied here relative to grain boundary conductivities (Eqs. 6 and 7).

A typical example of impedance spectra (Z—impedance) in complex form presentation ($-Z''$ *vs* Z', where Z''—Im Z, Z'—Re Z), recorded for $BaCe_{0.75}Zr_{0.1}Y_{0.15}O_{3-\delta}$ at 200 °C in dry oxygen atmosphere in a complex impedance representation, is reported in Fig. 2a. Representative spectra for $BaCe_{1-x}Zr_xYO_{3-\delta}$ are similar in their general form to spectra for samples with protonic conductivity prepared by both sol-gel and other routes reported elsewhere [25, 26]. The large grain-boundary response and the depressed low frequency arc were observed by other authors as well for samples of $Ba_xCe_{0.64}Zr_{0.2}Nd_{0.1}O_3$, $Ba_xCe_{0.64}Zr_{0.2}Gd_{0.1}O_3$ and $BaCe_{0.7}Zr_{0.1}Y_{0.2}O_{3-\delta}$ made by solid state routes [17, 27, 28]. This behaviour was generally accepted to attribute the differences in ceramic microstructures. To a first approximation, the diameter of each arc corresponds to one of the three regions of the materials (named also as grain interior, grain boundary and electrode) and should be referred to its resistance. Complex impedance plots ($-Z''$ *vs* Z'), which highlights the resistive impedance components, show a variations of about two-three order of magnitude during the increasing of the temperature up to 300 °C. The capacitance of any components depends on the relative permeability of material and on the geometric dimensions of the regions. Similarly to other solid electrolytes, the obtained C values for $BaCe_{1-x}Zr_xYO_{3-\delta}$ oxides associated with bulk component

were at least two orders of magnitude lower than that for grain boundary or surface components. The capacitance of the interior conductivity was found to change from 3.4×10^{-11} F to 4.9×10^{-10} F in dry oxygen atmosphere between 100 and 200 °C and conserved this value ($\sim 10^{-10}$ F) up to temperatures where bulk and grain boundary contributions may be separated. The differences in C at lowest temperatures were probably strongly related to the difficulties in the separation of two contributions and often underlined in literature. Since the capacitance of any components reflects the relative permeability of material and the geometric dimensions of the region associated, the identification of the impedance arcs in the complex impedance representation was achieved by considering the magnitude of the associated C [23]. In addition to the capacitance, R_1, R_2, f_{rel} and τ (f_{rel} is relaxation frequency and τ is the time constant, $2\pi f_{rel}\, RC = 2\pi f_{rel}\tau = \omega\tau = 1$) were extracted by impedance spectroscopy spectra. As known, the time constant τ is an intrinsic property and is independent of the geometry of the region involved. Spectroscopic plots of imaginary part of impedance (Z'' vs f) under dry oxygen (Fig. 2b) and nitrogen for $BaCe_{0.75}Zr_{0.1}Y_{0.15}O_{3-\delta}$ show two well defined maxima situated at two distinguished frequencies. The values of the frequencies associated with maxima in Z'' correspond to the relaxation frequencies, f_{rel}, of the bulk and grain boundary regions. At 200 °C, $f_{rel\ bulk} \approx 391$ kHz, $f_{rel\ gb} \approx 2.8$ kHz indicating an increase of the τ from $\approx 4 \times 10^{-7}$ to

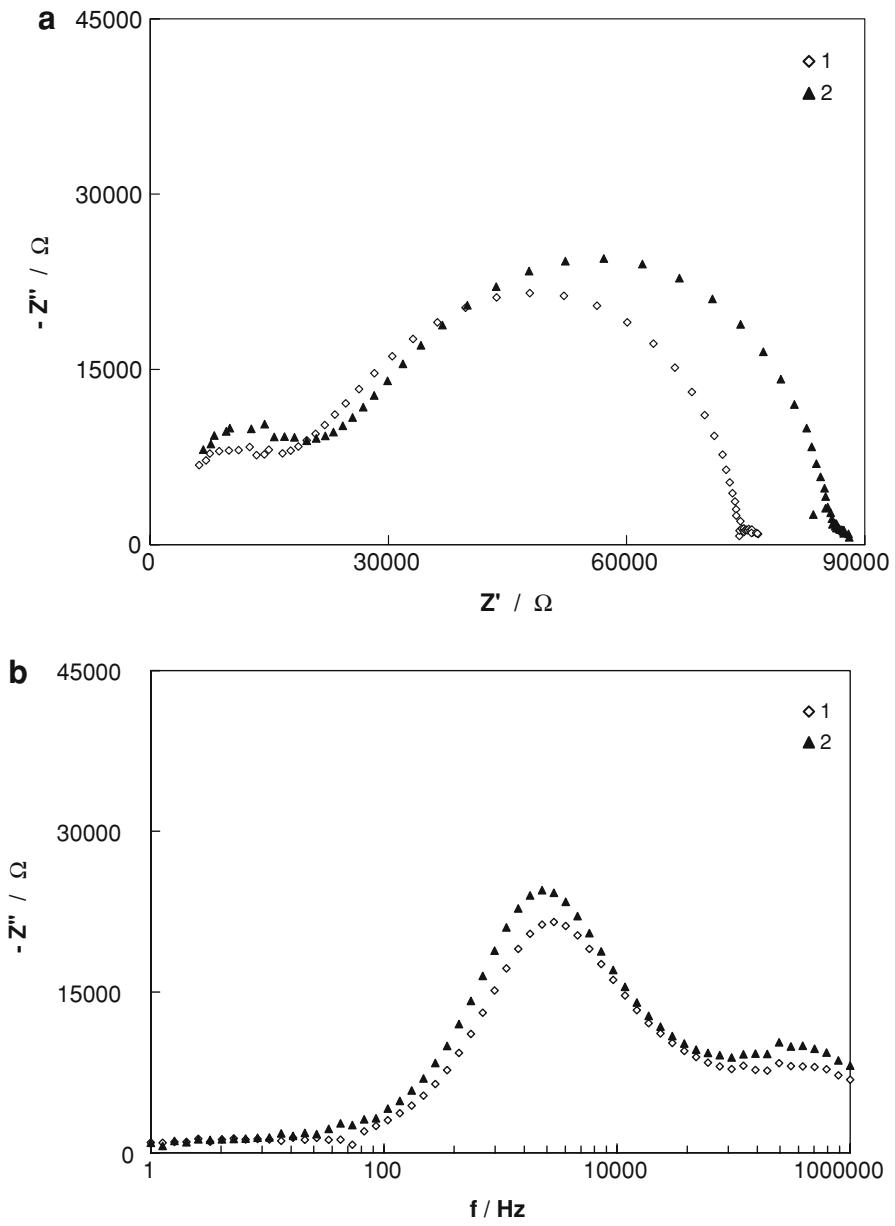

Fig. 2 $BaCe_{0.75}Zr_{0.1}Y_{0.15}O_3$ solid solution **a** complex impedance and **b** spectroscopic Z'' vs log f plots measured from 1 Hz to 1 MHz at 200 °C in different oxygen atmosphere: (1) dry, (2) wet ($P_{H_2O} = 0.5$ bar)

$\approx 5 \times 10^{-5}$ s. The position and the magnitude of each of them are changed with the increasing of temperature.

After heating from 100 to 900 °C in dry oxygen atmosphere for two consecutive times, the water (0.5 bar) was added in the oxygen flowing gas. Collected experimental data in wet oxygen show a relative small variations in both bulk and grain-boundary regions (Fig. 2a, b). A small increasing both in R_1 and R_2 were accompanied with shift of $f_{\text{rel gb}}$ from 2.8 to 2.3 kHz. The bulk f_{rel} did not change. The conductivity of $BaCe_{0.75}Zr_{0.1}Y_{0.15}O_{3-\delta}$ measured in dry oxygen (Fig. 1a) below the 500 °C was some higher than that in wet oxygen at low temperature. This tendency could be explained by the defect equilibrium chemistry [11, 29]. The conductivity of the $BaCe_{0.75-x}Zr_xY_{0.15}O_{3-\delta}$ at 500 °C and 700 °C measured in dry and wet O_2 atmospheres is reported in Table 1. The good linear correlation ($R^2 = 0.9978$) between the total conductivity ($\sigma_{\text{tot}}T$) and 1,000/T (curve 2 in Fig. 1a) under dry O_2 condition occurs in the whole 100–900 °C temperature range. Better linearization of the Arrhenius plot for $BaCe_{0.75}Zr_{0.1}Y_{0.15}O_{3-\delta}$ was obtained in temperature range from 100 to 400 °C ($R^2 = 0.9996$).

The total conductivities measured in N_2 dry gas atmosphere (oxygen partial pressure in N_2 gas $<10^{-7}$ bar) for $BaCe_{0.75}Zr_{0.1}Y_{0.15}O_{3-\delta}$ pellet are reported in Fig. 1b. The total conduction in flowing dry nitrogen decreases with respect to that in dry oxygen since concentration of holes is supposed to be small at low p_{o_2} (neglecting any contribution due to electronic defects).

After two consecutive heating from 100 to 900 °C in dry nitrogen atmosphere, the impedance data for $BaCe_{0.75}Zr_{0.1}Y_{0.15}O_{3-\delta}$ were collected in flowing wet nitrogen (0.5 bar H_2O) too. Resulting σ_{tot} slightly increases with respect to that in dry conditions (Fig. 1b, Table 1). A relatively small variations were found also at high frequencies in bulk contributions ($f_{\text{rel}} \approx 625$ kHz), while strong influences were observed in the low frequency range in grain-boundary contributions. (In dry condition $f_{\text{rel}} \approx 23.5$ kHz, under wet nitrogen $f_{\text{rel}} \approx 7.3$ kHz). Larger deviations from single Arrhenius plot in dry N_2 atmosphere with respect to that in dry O_2 were observed at the temperatures above 500 °C.

Table 1 Comparison of total conductivity of $BaCe_{0.75-x}Zr_{0.1}Y_{0.15}O_3$ solid solution in dry and wet oxygen, nitrogen and hydrogen atmospheres at 500 °C and 700 °C

Atmosphere	t (°C)	Total conductivity	
		$10^{-3} \times \sigma_{\text{Dry}}$ (S/cm)	$10^{-3} \times \sigma_{\text{WET}}$ (S/cm)
Oxygen	500	4.32	4.4
	700	21.70	22.0
Nitrogen	500	3.54	3.66
	700	7.4	8.98
Hydrogen	500	3.33	5.9
	700	6.8	19.5

As it is evident from Fig. 1a and b, in both dry gas atmospheres the repeated heating of $BaCe_{0.75}Zr_{0.1}Y_{0.15}O_{3-\delta}$ solid solution pellets produces the characteristic thermal hysteresis in total conductivity: retraces the high temperature portion of the curve, but proceeds different at low temperature. Similar behaviour was observed in dry air and dry helium atmospheres for Y-doped barium cerate ($BaCe_{0.9}Y_{0.1}O_{3-\delta}$) samples prepared from reactive ceramic powder (0.44 μm average particle size) by combustion spray pyrolysis and sintered at 1,450 °C temperature during 10 h (99% density) [25]. As it was observed early in [30] during the furnace cooling of $BaZr_{0.2}In_{0.8}O_{2.6}$ the insertion of water and/or oxygen could have varied the volume per formula unit. As a consequence, the thermal hysteresis could be noted. Complete dehydration in the present paper of $BaCeZrYO_{3-\delta}$ solid solutions were only observed at high temperature. The dehydrated condition then persisted back to low temperature and during next day repeating heating. (Above 600 °C in dry oxygen and above 500 °C in nitrogen). This is probably due to loss of holes and creation of vacancies by reverse of Wagner reaction and non regenerating of holes at the temperature below 500–600 °C [25]. Accordingly, the protonic carrier concentration of the ceramic electrolytes is determined by the degree of hydration, the limit of which is determined by the concentration of oxygen ion vacancies in the ("as-fired") ceramic, prior to hydration. When dehydration takes place, two protons and one oxygen ion become "true" water molecules as they desorbed from the surface of the ceramic into the gas phase. Thus, for Y doped barium cerate $BaCe_{0.9}Y_{0.1}O_{3-\delta}$ in dry air and dry helium atmospheres it was observed that the ceramic dehydration and generation of oxygen vacancies occurred by the reverse of Wagner reaction at about 600–650 °C and was not recuperated during the decreasing of the temperature [25]. Similar phenomena were found later for sol-gel prepared $BaCeY_yO_{3-\delta}$ solid solutions (~0.8 μm average particle size) sintered at 1,250 °C during heating cycles in oxygen dry atmosphere [29]. It is difficult to know where the water is resided. It was assumed in [31] that water is incorporated into the grains of the ceramics ($Ba_xCe_{0.64}Zr_{0.2}Nd_{0.1}O_3$ and $Ba_xCe_{0.64}Zr_{0.2}Nd_{0.1}O_3$), while in [32] were concluded that part of the water resided in BaO-rich grain boundary phases for $BaCeGdO_3$ ceramics both prepared by solid state reactions. There is no evidence, in the sol-gel $BaCeZrYO_{3-\delta}$ and $BaCeYO_{3-\delta}$ solid solutions prepared by sol-gel route, of any BaO-rich phase [18, 19].

It can been noticed from Table 1 that at 500 and 700 °C the conductivities of $BaCe_{0.75}Zr_{0.1}Y_{0.15}O_{3-\delta}$ in dry

Table 2 Comparison of the activation energy (E_a) and pre-exponential factor (σ_0) for the total conductivity in dry atmospheres

Atmosphere	t/°C	E_a (eV)	σ_0 (K S/cm)
Oxygen	100–400	0.723	2.1×10^5
Nitrogen	100–400	0.65	5.5×10^4
Hydrogen	100–400	0.653	5.8×10^4

atmospheres of both nitrogen and hydrogen were lower than that of oxygen, while in wet atmospheres the conductivity in hydrogen increases over of that oxygen and nitrogen. The activation energies in 100–400 °C temperature range for conduction in H_2 and N_2 in absence of water (reported in Table 2) were lower than that in O_2.

3.1.2 *Conductivity of $BaCe_{0.85-x}Zr_xY_{0.15}O_{3-\delta}$ in 5%H_2/Ar wet gas atmosphere*

It is known from scientific literature that structure of perovskite oxides is very sensitive to their composition. Pure $BaZrO_3$ is primitive cubic perovskite, group P*m3m*. With the introduction of Y^{3+} ions (0.93 Å) at the B-sites (0.80 Å for Zr^{4+} and 1.01 Å for Ce^{4+}), the BO_6 polyhedra may tilt and distort thus causing distortion of the lattice. For example, as it is noted in [27], the structure of $Ba_{0.97}Zr_{0.8}Y_{0.16}Zn_{0.04}O_3$ is primitive cubic, but the one with little more yttrium in the B-site, $Ba_{0.97}Zr_{0.77}Y_{0.19}Zn_{0.04}O_3$ is tetragonal. $BaCe_{0.9}Y_{0.1}O_{3-\delta}$ and $BaCe_{0.85}Y_{0.15}O_{3-\delta}$ spectra were indexed as orthorhombic crystal system, *Pnma* space group [6, 21]. In the case of $BaCe_{1-x-y}Zr_xY_yO_{3-\delta}$ solid solutions, the pseudo cubic lattice parameters show a distortion from a perfect cubic, which reduced with increasing of Zr content [18]. Pseudo cubic lattice constants, together with the cell volumes and distortion parameter (d.p.), were found to linearly decrease as Zr atomic percentage increase (Table 4).

The σ_{tot} for doped mixed oxides $BaCe_{0.85-x}Zr_xY_{0.15}O_{3-\delta}$ in the 100–900 °C temperature range were measured in flowing wet (0.5 bar H_2O) 5%H_2/Ar atmosphere, where the process of water vapour adsorption is supposed to take place and the reaction with oxygen ion vacancies produces hydroxide species (Eq. 1). The Arrhenius plots in wet 5%H_2/Ar atmosphere presented in Fig. 3a showed a marked curvature in slope around ~500 °C for all Zr contents. Good linear Arrhenius plots of σ_{tot} (shown in Fig. 6a, curves 1–5) for $BaCe_{0.85-x}Zr_xY_{0.15}O_{3-\delta}$ under wet 5%H_2/Ar conditions were found only in the temperature range from 100 to 300 °C ($R^2 = 0.9996$) (Table 5).

In wet 5%H_2/Ar the phenomena related to initial and second heating were measured for $BaCe_{0.75}Zr_{0.1}Y_{0.15}O_{3-\delta}$ (Fig. 3b). At 350 °C initial and repeating curves were superposed. Since at temperature around ~750 °C under flowing wet 5%H_2/Ar conditions occurs a marked curvature in slope of Arrhenius plots for all Zr contents (Fig. 3a) and visual drop of the measured conductivity at higher temperatures (Fig. 3b), the repeat heating experiments were limited only to that composition.

The dependence of the total conductivities on x, at various temperatures is shown in Fig. 4. Among the specimens examined, the conductivity slightly decreases from $x = 0$ to $x = 0.2$, and then remains rather stable up to $x = 0.4$. The conductivity values for $BaCe_{0.65}Zr_{0.2}Y_{0.15}O_{3-\delta}$ collected in wet hydrogen atmosphere at 500 °C is 5.90×10^{-3} S cm^{-1}. At 700 °C the conductivity values were measured at 2.51×10^{-2} S cm^{-1} for $x = 0$, 1.9–2×10^{-2} S cm^{-1} for $x = 0.1$ and decrease up to 1.35×10^{-2} S cm^{-1} for $x = 0.3$. Fabbri et al. [16] studied the conductivity and activation energy of $BaCe_{0.8-x}Zr_xY_{0.2}O_{3-\delta}$ (from $x = 0$ to $x = 0.8$) prepared in a similar way using sol-gel synthesis and sintering temperature at 1,550–1,650 °C. The high temperature total conductivity in wet (0.03 atm H_2O) hydrogen atmosphere, reported in [16], was something lower than that has been obtained in this work. At 700 °C the conductivity values reported are 1.14×10^{-2} S cm^{-1} for $x = 0$, and 7×10^{-3} S cm^{-1} for $x = 0.3$. Zuo [17] studied the conductivity of $BaCe_{0.7}Zr_{0.1}Y_{0.2}O_{3-\delta}$ prepared by solid state reaction method and sintering temperature at 1,550–1,650 °C. The highest conductivity (2.0×10^{-2} S cm^{-1} at 700 °C) were obtained in wet (0.03 atm H_2O) 4%H_2/N_2 for $BaCe_{0.7}Zr_{0.1}Y_{0.2}O_{3-\delta}$ pellets. In the present studies, on the repeating of preparation steps, the regular decreasing of the porosity during sintering procedures and the corresponding increasing of the sample density were always observed. As a consequence, good reproducible of the impedance responses were also found. High reproducibility of the ceramic properties for the $BaCe_{0.85-x}Zr_xY_{0.15}O_{3-\delta}$ studied in this work evidently relates to preparation route, to the specific features of the structure of the initial powder (foamed structures of 100–300 nm sizes aggregated in open, sponge-like structures) and to the pore shapes and their distribution. Strong chelating power of EDTA used in this synthesis proved to promote the uniformity of the metal ion distribution and affect the powder morphology [18].

In Table 3, the activation energies and the pre-exponential factors for $BaCe_{0.85-x}Zr_xY_{0.15}O_{3-\delta}$ are confronted for the total conductivity in wet 5%H_2/Ar atmosphere in 350–600 °C temperature range.

In order to characterize highly resistive grain boundary ceramics, as it was proposed in [24, 33, 34], bulk and grain boundary contributions to the total electrical properties were separated in low (100–250 °C) and high (300–600 °C) temperature range. Even in the absence of second phases detected by XRD, the electrical properties of grain

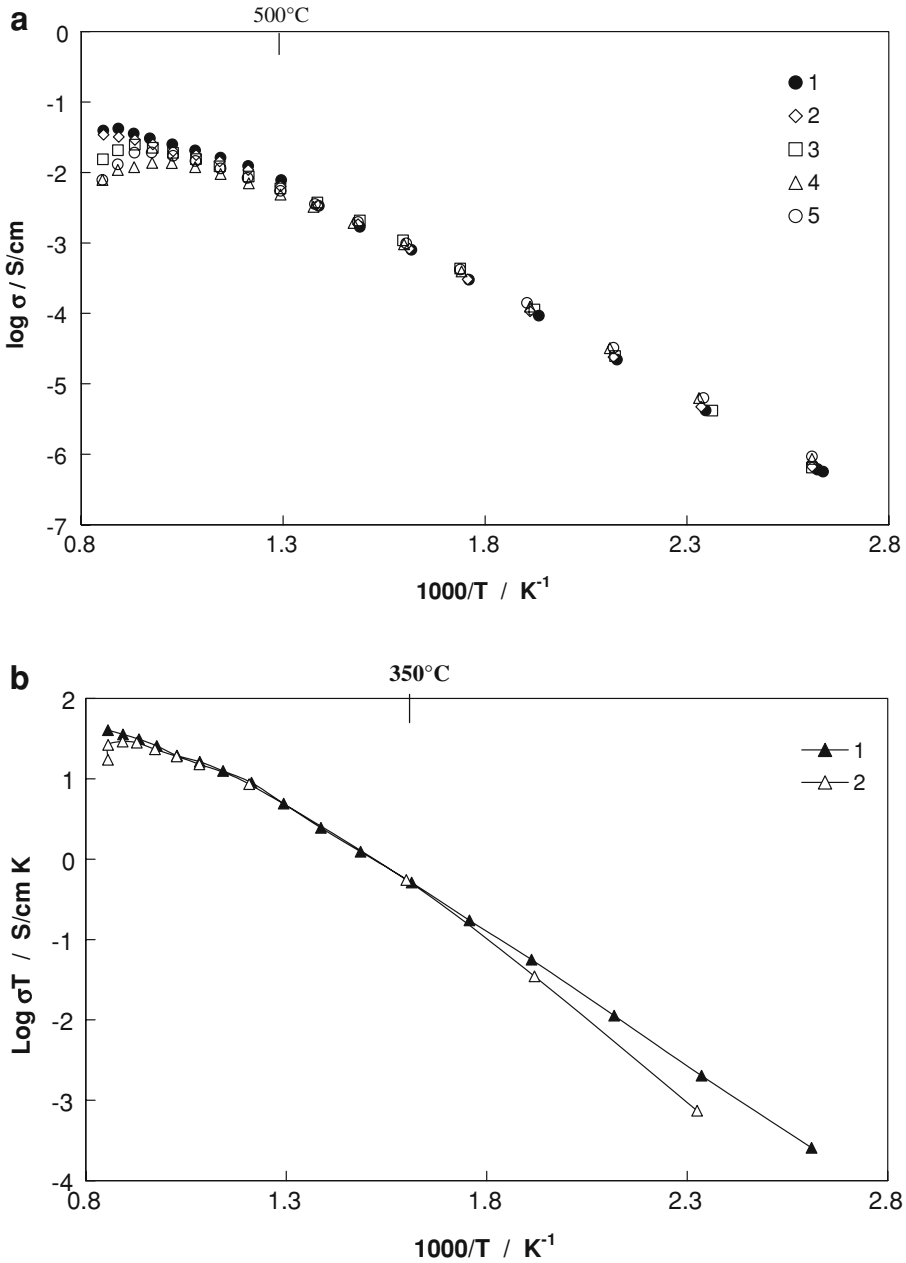

Fig. 3 Arrhenius plots of total conductivity in humidified 5%H_2/Ar atmosphere ($P_{H_2O} = 0.5$ bar) measured for solid solutions: **a** $BaCe_{0.85-x}Zr_xY_{0.15}O_3$, x: (1) 0; (2) 0.1; (3) 0.2; (4) 0.3; (5) 0.4; **b** $BaCe_{0.75}Zr_{0.1}Y_{0.15}O_3$ (1) first heating (2) second heating

boundary regions have a dominant effect on the impedance spectra. In Fig. 5a, b, the impedance data recorded in wet 5%H_2/Ar atmosphere for $BaCe_{0.85-x}Zr_xY_{0.15}O_3$ solid solutions in the low temperature range (where this separation is still possible) are reported in both complex impedance (Z'' *vs* Z') and spectroscopic (Z'' *vs* log *f*) plot representations. The complex impedance plots collected in Fig. 5a, show strongly blocking grain boundaries in wet 5%H_2/Ar atmosphere at 154 °C for solid solutions with $x = 0$ and $x = 0.1$, which became comparable with that of the bulk for $x = 0.3$ and smaller for $x = 0.4$. The same trends are evident for all recorded spectroscopic plots (shown at 110 °C in Fig. 5b): the magnitude of Z'' decreases with Zr content up to $x = 0.4$. The relaxation frequency of bulk is ≈46.7 kHz ($\tau \approx 3.4 \times 10^{-6}$ s) and that of grain boundary ≈275 Hz ($\tau \approx 5.8 \times 10^{-4}$ s) remain constant. From the impedance dependences measured in wet 5%H_2/Ar and collected in Fig. 5a, b it is apparent that relation between magnitudes of Z_{bulk}'' and Z_{gb}'' starting from $x = 0.3$ shifts in favour of bulk contribution. Although grain boundary geometry (in sense of R and C) changes with respect to x at each temperature (at 154 °C parameter (Q) varies from 6×10^{-10} F for $x = 0.1$ to 1.34×10^{-9} F for $x = 0.4$), the relaxation frequency

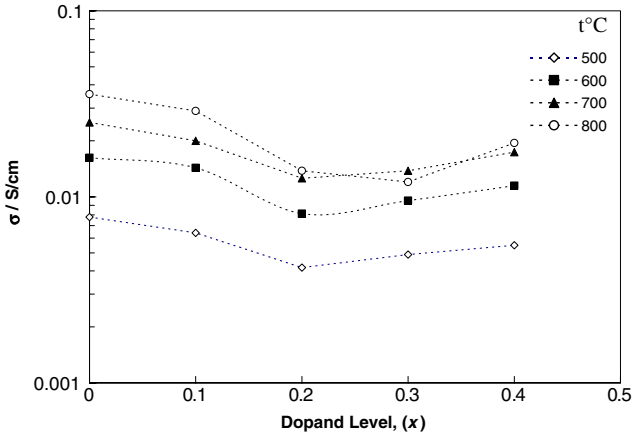

Fig. 4 Isothermal conductivities at 500, 600, 700 and 800 °C as a function of dopand level x for the $BaCe_{0.85-x}Zr_xY_{0.15}O_3$ samples (measured in 5%H_2/Ar, $P_{H_2O} = 0.5$ bar)

Table 3 Comparison of the activation energy (E_a) and pre-exponential factor (σ_0) for the total conductivity in wet 5%H_2/Ar atmosphere in 350–600 °C temperature range

Y%	%Zr	350–600 °C	
		E_a (eV)	σ_0 (K S/cm)
15	0	0.405	3.066×10^3
15	10	0.599	1.125×10^4
15	20	0.521	1.109×10^4
15	30	0.500	6.248×10^3
15	40	0.521	1.049×10^4

does not, indicating that the nature of the transport process phenomena in the grain is not significantly altered by increasing of the Zr contents.

Using simple brick layer model and assuming that dielectric constant of the grain boundary is approximately equal to that of the bulk, both contributions to the total conductivity were calculated for the $BaCe_{0.85-x}Zr_xY_{0.15}O_3$ solid solutions. With respect to this approximation, the grain boundary resistivity and thickness were deduced from fit of the experimental data to equivalent circuits described below. Bulk and grain boundary elements (represented as Q_1, Q_2, where Q is constant phase element since impedance arcs were depressed, $C = (R^{1/n-1})\ Q^{1/n}$ for $BaCe_{0.85-x}Zr_xY_{0.15}O_3$ oxides show pF and nF geometrical capacitance, while the electrode elements has μF capacitance. The frequently reasonable approximation provided that the grain boundary properties are laterally homogeneous and do not vary from boundary to boundary. Partial electrical grain boundary conductivities could be calculated also in two ways. The first is to convert the resistance to the conductivity by consideration of sample geometry: Eqs. 4 and 5. This simple model was applied for the total conductivity calculations in oxygen, nitrogen and 5%H_2/Ar atmospheres (Fig. 1a, b, 3a, b and 6a). In the same approximations, the apparent (or macroscopic) grain boundary conductivity ($\sigma_{gb_{app}}$) can be calculated on the base of overall sample geometry and measured grain boundary resistances. $\sigma_{gb_{app}}$ for the $BaCe_{0.85-x}Zr_xY_{0.15}O_3$ ($x = 0.1$, 0.2, 0.3 and 0.4) are shown in Fig 6b. Another way takes into account the real grain boundary area, grain boundary size including grain boundary layer thickness. The specific grain boundary conductivity $\sigma_{gb\ spec}$ can be defined as

$$\sigma_{gb\ spec} = \sigma_{gb} d/L = 1/R_{gb} \times l/A \times d/L. \quad (6)$$

Since the grain boundary thickness d and grain size L were not known, $\sigma_{gb\ spec}$ were calculate using RC method and the brick layer model [22, 35, 36]

$$\sigma_{gb\ spec} = l/A \cdot (C_{bulk}/C_{gb}) \cdot 1/R_{gb} \quad (7)$$

The impedance data were fitted to an equivalent circuit consisting of two or three serial RQ elements (R_1, Q_1, R_2, Q_2, R_3, Q_3), the fit results were evaluated on the basis of standard deviations and percentage errors for each element. If the high frequency arc is fitted to a resistor (R_1) in parallel with a Q_1, n values of ca. 0.96–0.98 under the wet 5%H_2/Ar were observed. R_3, Q_3 represent the interface electrode/electrolyte. The impedance variation can be modelled as a charge transfer resistance (R_3) in parallel to the CPE element (Q_3) and/or Warburg component related to mass transport phenomena at this interface and varying with diffusion of H^+ through a concentration gradient near the electrode. This contribution will not be considered in following discussion. As an example the fitting results of impedance data recorded for $BaCe_{0.85-x}Zr_xY_{0.15}O_3$ ($x = 0.4$) at 154 °C is reported in Fig. 5a, where the experimental data (points) in complex plot presentation are compared with fit results (lines), revealing a very good agreement both for weight unit and modulus calculations. For the purpose of this study, the unit-weight calculation was mostly used.

The σ_{total} for the $BaCe_{0.85-x}Zr_xY_{0.15}O_3$ (x from 0.1 to 0.4) measured in wet hydrogen atmosphere and low temperature range are compared in Fig. 6a (in Arrhenius plot presentations) to those of bulk (σ_{bulk}) both calculated on the base only of the geometric sample dimensions. Due to the non perfect linearity of the Arrhenius plots of total, bulk and grain boundary conductivities the activation energy values together with the pre-exponential factors are dependent on the number of points (temperatures) used in the linear fittings. The experimental data collected in Fig. 6a were limited to 100–250 °C interval (were the arcs in complex impedance plots are at least partially resolved). With increasing of bulk Zr concentration and temperature in that temperature range, the differences between total and bulk conductivities become smaller and smaller. The grain boundary conductivity $\sigma_{gb\ sp}$ (Fig. 6c) is lower than that of

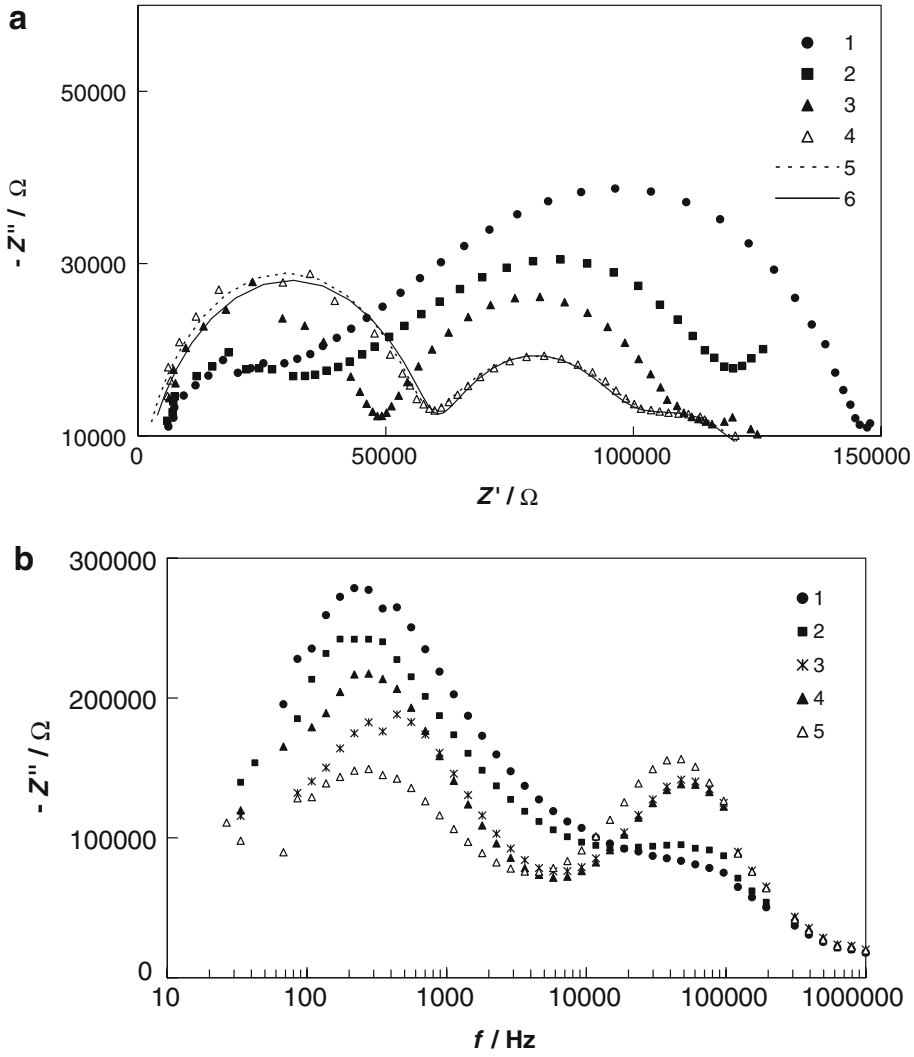

Fig. 5 $BaCe_{0.85-x}Zr_xY_{0.15}O_3$ impedance data measured in humidified 5%H_2/Ar atmosphere ($P_{H_2O} = 0.5$ bar) from 1 MHz to 1 Hz at various temperatures in: **a** complex impedance plot presentation at 154 °C; Zr content *x*: (1) 0; (2) 0.1; (3) 0.3; (4) 0.4; (5) fit Unit-Weight; (6) fit Calc-Modulus. **b** spectroscopic (Z″ vs log *f*) plot presentation at 110 °C: (1) 0; (2) 0.1; (3) 0.2 (4) 0.3; (5) 0.4

the bulk σ_{bulk} (Fig. 6a) in the whole low temperature range (100–350 °C).

In Table 4 are collected the activation energies and the pre-exponential factors determined for the bulk and grain boundaries at low temperature range (100 °C < T ≤ 250 °C) and sample compositions, densities pellet geometric constants and lattice parameters. The bulk activation energies ($E_{a\ bulk}$) vary from 0.5 eV to 0.605 eV for BaCe $Zr_xY_{0.15}O_{3-\delta}$ when *x* increase from 0 to 0.4. The bulk pre-exponential factor decreases from 1.4×10^3 K S/cm when *x* changes from 0 to 0.1 and (1.91×10^2 K S/cm ($x = 0.1$) and remains close to $\sim 10^2$ K S/cm for all other compositions. In contrast, the grain boundary activation energies vary in much more narrow range (0.836–0.877 eV) when *x* increase from 0.1 to 0.4 and rapidly decreases when *x* changes from 0 to 0.1. The grain boundary pre-exponential factors of $BaCe_{0.85-x}Zr_xY_{0.15}O_{3-\delta}$ is about too order of magnitude higher than that of all bulk ones for all samples.

In contrast to the pre-exponential factor, which is almost similar for *x* 0.1, the bulk activation energies are clearly proportional to the lattice parameters. The $BaCe_{0.85-x}Zr_x$ $Y_{0.15}O_3$ samples with large lattice parameters and bigger distortion parameter (d.p.) have the smaller bulk activation energies. This result is in agreement with the literature data on $BaZr_xY_yO_{3-\delta}$ [37].

Considering the grain boundaries, the apparent and the specific grain boundary conductivities are plotted as a function of the inverse temperature in Fig. 6b, c. The ratio of capacitance (C_b/C_{gb}) at 250 °C used to obtained specific grain boundary conductivities are shown in Table 4. In comparison to the apparent grain boundary conductivities, the specific grain boundary conductivities is ∼two order of magnitudes lower over the temperature range 100–250 °C.

The Zr introduction into Y-doped $BaCeO_3$ structure enhanced the chemical stability solid solutions in CO_2 and H_2O environments [18, 19]. The transition from predominantly unstable to mainly stable oxides was observed for the $BaCe_{0.85-x}Zr_xY_{0.15}O_3$ solid solutions having Zr content $x > 0.2$. For the $BaCe_{0.85-x}Zr_xY_{0.15}O_3$ compositions the impedance investigations show (C_b/C_{gb}) ratio (and in

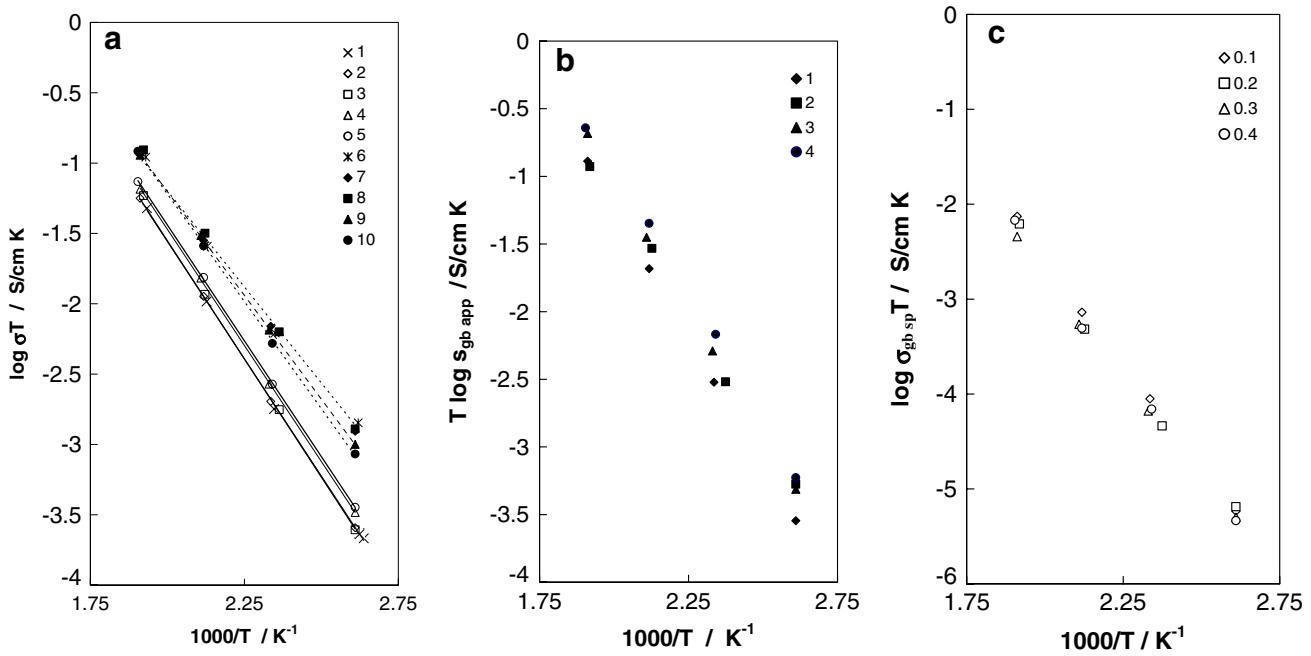

Fig. 6 Arrhenius plots of conductivities for the $BaCe_{0.75}Zr_{0.1}Y_{0.15}O_3$ solid solutions in humidified $5\%H_2/Ar$ atmosphere ($P_{H_2O} = 0.5$ bar) **a** total (σ_{total}), *x*: (1) 0; (2) 0.1; (3) 0.2; (4) 0.3; (5) 0.4; bulk (σ_{bulk}), *x*: (6) 0; (7) 0.1; (8) 0.2; (9) 0.3; (10) 0.4; **b** apparent grain boundary ($\sigma_{gb_{app}}$), *x*: (1) 0.1; (2) 0.2; (3) 0.3; (4) 0.4. **c** specific grain boundary ($\sigma_{gb\ spec}$), *x*: (1) 0.1; (2) 0.2; (3) 0.3; (4) 0.4

consequence space-charge layer thickness δ) strongly decrease with *x* in wet $5\%H_2/Ar$ atmosphere.

In order to characterize the space-charge layers for the $BaCeZr_xY_{0.15}O_3$ solid solutions which is formed on grain-to-grain interface, the space-charge layer thickness ($\delta/L \sim C_b/C_{gb}$) for various *x* were calculated using the model described in [30], where the electrical properties of the grain boundaries of doped zirconia and ceria were reviewed in view of grain-boundary blocking effect, ionic transport across the grain boundaries and grain to-grain contact. On the basis of the model described there, the space-charge layer thickness (δ) of grain-to-grain contact was calculated. The results of these evaluations are presented in Table 5. The thickness of total space-charge layer, which is responsible of grain-boundary blocking effect, for $BaCeZr_xY_{0.15}O_3$ solid electrolytes, was found to vary with Zr content. Calculated δ has a nano scale magnitude in the 100–300 °C temperature range and decreases at 100 °C from 15 to 8 nm with increasing x from 0.1 to 0.4. This tendency conserves at increasing temperature.

4 Conclusions

On the base of these experimental observations, it is concluded that impedance techniques provide useful information on conductivity of doped barium cerate proton conductors $BaCe_{0.85-x}Zr_xY_{0.15}O_3$ ($x = 0, 0.1, 0.2, 0.3, 0.4$) obtained by a modified sol-gel Pechini process. Single phase perovskite nano-structured sub-micrometric $BaCe_{0.85-x}Zr_xY_{0.15}O_3$ pellets having high and reproducible densities (up to ~97%) were used in this work for the impedance investigations in both reductive and oxidative atmospheres. The activation energies for the conduction processes were comparable to those reported for similar proton conducting materials and decreases from 0.723 eV in dry oxygen to 0.65 eV in dry nitrogen. The introduction of Zr into the Y-doped $BaCeO_3$ structure decreases linearly the pseudo-cubic lattice constants at room temperature while the diffusion processes in the boundaries of grains in the low temperature range from 100 to 300 °C reflect the bulk Zr percentages in more complicated way: the $BaCe_{0.85-x}Zr_xY_{0.15}O_3$ solid solutions having Zr content $x \approx 0.2$–0.4 and $Y = 0.15$ were demonstrated high proton conductivities which are only slightly influenced by the Zr amount. In fact, as an example, the total conductivity at 500 °C under humidified $5\%H_2/Ar$ changed from 7.78×10^{-3} to 5.48×10^{-3} S/cm while varying the Zr content from 0 to 0.4. Comparison with the literature showed the crucial role of the synthetic method, the processing conditions and the barium excess on the materials properties. Therefore, these perovskite oxides seem to be promising candidates as electrolytes in hydrocarbon fuelled proton conducting inter-medium temperature SOFCs. One

Table 4 Comparison of the sample composition, density, pellet geometric constant, lattice parameters, unit cell volume of the sintered pellets with the activation energy (E_a) and pre-exponential factor (σ_0) for the bulk and grain boundary conductivity in wet 5%H_2/Ar atmosphere in 100–250 °C temperature range

Y%	%Zr	Density (%)	Cell const k = *l*/*A* (cm)	T_{sint} (°C)	Structure type	a (Å)	b (Å)	c (Å)	d.p.	V (Å^3)	Bulk		Grain boundary			C_b/C_{gb}	δ
											E_a (eV)	σ_0 (K S/cm)	E_a (eV)	$\sigma_{0\,gb_{app}}$ (K S/cm)	$\sigma_{0\,gb\,sp}$ (K S/cm)	250 °C	
																$\times 10^{-2}$	nm
15	0	89	0.6334	1250	Orthorombic					339.61	0.5	1.4×10^3	1.033		7.6×10^5	8	
15	10	95.8	0.6120	1300	Pseudo cubic	4.41	4.37	4.37	0.942	336.37	0.557	1.91×10^2	0.877	2.4×10^6	3.41×10^4	5.6	48.8
15	20	93	0.704	1400	Pseudo cubic	4.39	4.35	4.35	0.938		0.573	2.44×10^2	0.874	5.7×10^6	3.48×10^4	3.8	30
15	30	93	0.7205	1400	Pseudo cubic	4.36	4.32	4.33	0.934		0.586	1.3×10^2	0.836	3.1×10^6	3.23×10^4	2.18	26.3
15	40	94.4	0.6960	1450	Pseudo cubic	4.31	4.31	4.315	0.93	322.39	0.605	1.45×10^2	0.876	2.5×10^6	3.03×10^4	2.95	29.6

Table 5 Space-charge layer thickness (δ) calculated for different Zr contents x in the 110–300 °C temperature range

$BaCe_{0.75-x}Zr_xY_{0.15}O_3$	δ_{gb}/nm				
x	110 °C	150 °C	200 °C	250 °C	300 °C
0.1	17.3	25.3	29.7	48.8	169.4
0.2	14	18.3	16.5	30	82.6
0.3	12.4	15.5	18.3	26.3	55.3
0.4	7.8	10.2	11	29.6	39.7

outcome of this work will be the optimization of suitable anodic and cathodic materials in order to produce an anode-supported proton conducting IT-SOFC.

Acknowledgement This work has been supported by the "Celle a combustibile ad elettroliti polimerici e ceramici: dimostrazione di sistemi e sviluppo di nuovi materiali" FISR Project of MUR.

References

1. Iwahara H (1995) Solid State Ionics 77:289
2. Iwahara H, Asakura Y, Katahira K, Tanaka M (2004) Solid State Ionics 168:299
3. Kreuer KD (2003) Ann Rev Mater Res 33:333
4. Kreuer KD (1999) Solid State Ionics 125:285
5. Norby T (1999) Solid State Ionics 125:1
6. Chiodelli G, Malavasi L, Tealdi C, Barison S, Battagliarin M, Doubova L, Fabrizio M, Mortalò C, Gerbasi R (2009) J Alloy Compd 470:477
7. Glöckner R, Islam MS, Norby T (1999) Solid State Ionic 122:145
8. Grover Coors W, Readey DW (2002) J Am Ceram Soc 85:2637
9. Nowick AS, Du Y (1995) Solid State Ionics 77:137
10. Malavasi L, Ritter C, Chiodelli G (2008) Chem Mater 20:2343
11. Ma G, Matsumoto H, Iwahara H (1999) Solid State Ionics 122:237
12. Haile SM, Staneff G, Ryu KH (2001) J Mater Sci 36:1149
13. Katahira K, Kohchi Y, Shimura T, Iwahara H (2000) Solid State Ionics 138:91
14. Pechini MP (1967) U.S. Patent 3 330:697
15. Zha S, Fu Q, Lang Y, Xia C, Meng G (2001) Solid State Ionics 47:351
16. Fabbri E, D'Epifanio A, Di Bartolomeo E, Licoccia S, Traversa E (2008) Solid State Ionics 179:558
17. Zuo C, Zha S, Lui M, Hatano M, Uchiyama M (2006) Adv Mater 18:3318
18. Barison S, Battagliarin M, Cavallin T, Doubova L, Fabrizio M, Mortalò C, Boldrini S, Malavasi L, Gerbasi R (2008) J Mater Chem 5120
19. Barison S, Battagliarin M, Cavallin T, Daolio S, Doubova L, Fabrizio M, Mortalò C, Boldrini S, Gerbasi R (2008) Fuel cells 5:360
20. Kruth A, Irvine JTS (2003) Solid State Ionics 162–163:83
21. Ryu KH, Haile SM (1999) Solid State Ionics 125:355
22. Barsukov E, Macdonald JR (eds) (2005) Impedance spectroscopy: theory, experiment and application. Wiley, Hoboken, New-Jersey
23. Fletcher JG, West AR, Irvine JTS (1995) J Electrochem Soc 142:2650
24. Imashuku S, Uda T, Nose Y, Kishida K, Harada S, Innui H, Awakura Y (2008) J Electrochem Soc 155:B581

25. Groover W, Swartzlander R (2005) Proceeding of the 26th Riso International Symposium on Material Science: Solid State Electrochemistry, Ed. National Laboratory, Roskilde, Denmark, p 185
26. Zhong Z (2007) Solid State Ionic 178:213
27. Tao S, Irvine JTS (2007) J Solid State Chem 180:3493
28. Ma G, Shimura T, Iwahara H (1999) Solid State Ionics 97:103
29. Boldrini S, Barison S, Doubova L, Mortalò C, Fabrizio M (2009) Fuel Cells (submitted)
30. Goodenough JB, Manthiram A, Kuo J-F (1993) Mater Chem Phys 35:221
31. Bonanos N, Knight KS, Ellis B (1995) Solid State Ionics 79:161
32. Kreuer KD, Schönherr E, Maier J (1994) State Ionics 70/71:278
33. Babilo P, Uda T, Haile SM (2007) J Mater Res 22:1322
34. Tian C, Chan S-W (2000) Solid State Ionics 134:89
35. Lai W, Haile S (2005) J Am Ceram Soc 88:2979
36. Su X-T, Yan Q-Z, Ma X-H, Zhang WF, Ge C-C (2006) Solid State Ionics 177:1041
37. Duval SB, Holtappels P, Stimming U, Graule T (2008) Solid State Ionics 179:1112